Available online at www.sciencedirect.com

ScienceDirect

journal homepage: http://www.elsevier.com/locate/acme

Original Research Article

Explorative study of rotary tube piercing process for producing titanium alloy thick-walled tubes with bi-modal microstructure

Zhe Zhang [a], *Dong Liu* [a,*], *Yanhui Yang* [a], *Yong Zheng* [a], *Yuhua Pang* [b], *Jianguo Wang* [a], *Haiping Wang* [a]

[a] *School of Materials Science and Engineering, Northwestern Polytechnical University, Xi'an 710072, China*
[b] *School of Metallurgical Engineering, Xi'an University of Architecture and Technology, Xi'an 710055, China*

ARTICLE INFO

Article history:
Received 8 February 2018
Accepted 20 May 2018
Available online 29 June 2018

Keywords:
Rotary tube piercing
Titanium alloy
Thick-walled tube
FEM

ABSTRACT

In order to solve the existing problems in the manufacturing of titanium alloy thick-walled tubes (TATWs), an innovative plastic forming method for the preparation of TATWs using rotary tube piercing (RTP) process was studied. In this paper, the advantages and basic principles of the RTP process were described. A new finite element model is established to study the effect of the thermal parameters on the RTP process of TATWs. Based on the control variable method, two key problems of rolling block and severe temperature rise in the RTP process were all solved, and the TATWs with bi-modal microstructure were produced by the self-developed piercing mill. In addition, the microstructure uniformity of the pierced tube was analyzed. Based on the experimental and numerical investigations, it's found that the RTP process is a viable process for manufacturing TATWs with bi-modal microstructure.

1. Introduction

As a billet for producing hollow structural parts, many titanium alloy thick-walled tubes (TATWs) are demanded in aeronautics, astronautics, energy power, transportation and petrochemical industry [1,2]. Because of the excellent comprehensive performance of bi-modal microstructure, the demand for TATWs with bi-modal microstructure is most urgent [3]. Three methods are most commonly used to produce TATWs: punching, drawing [4] and extrusion [5]. However, these three methods have the following disadvantages: (1) large forming load; (2) low processing efficiency; (3) low utilization of materials; (4) complex manufacturing process [6]. In view of the current processing methods, the demand for modern industrial manufacturing is difficult to meet. Therefore, it is of great significance to develop an advanced processing technology to manufacture TATWs.

Rotary tube piercing (RTP) is an innovative plastic forming process which relies on local and incremental plastic deformation to transform solid billets into hollow tubes. Many scholars have conducted extensive research on the theoretical

* *Corresponding author.*
E-mail addresses: 15891769371@126.com (Z. Zhang), liudong@nwpu.edu.cn (D. Liu).
https://doi.org/10.1016/j.acme.2018.05.005

research of RTP process, due to the main advantages of its small forming load, high production efficiency, and high material utilization rate. Romanenko [7] and Zhao [8] studied the evolution law of tube dimension, and proposed adjusting the plug position to improve the dimensional stability of tube. Skripalenko [9] discussed the influence of plug shape on central damage, and Bariani further [10] predicted the crack position of the billet. What's more, Liu et al. [11] performed an experiment on the RTP process of stainless steel, and concluded that shear stress is the reason for the separation defect.

About the application of RTP process to the preparation of TATWs, the predecessors have done some exploratory research. Yajing et al. [12] obtained the Ti–6Al–4V alloy thin-walled tubes at 980 °C, and the ratio (length–diameter) of pierced tubes is about 10. The pierced tube consisted of the fully lamellar alpha microstructure within the beta matrix (widmanstatten microstructure). Jiming et al. [13] found that the optical micrograph map of Ti–6Al–4V alloy tubes obtained at 980 °C is the coarse lamellar alpha microstructure within the beta matrix (widmanstatten microstructure), and the ratio (length–diameter) of pierced tubes is about 10. In summary, the previous experiments were all carried out at higher temperature to ensure the smooth piercing of titanium alloy tube, which leads to the optical micrograph map of the pierced tube was widmanstatten microstructure. The plasticity and toughness of widmanstatten microstructure are poor, which is not conducive to the subsequent processing of hollow structural parts. The bi-modal microstructure, which has excellent comprehensive performance, is the goal we pursue. In addition, previous works can only produce titanium alloy tubes with a ratio (length–diameter) of 10, and there is no report on the thick-walled tubes with a ratio (length–diameter) less than 5. Compared with the thin-walled tubes, the internal expansion of thick-walled tubes is smaller and thus the phenomenon of rolling block is more likely to occur. In this paper, the factors affecting the piercing process are systematically analyzed to obtain the TATWs with bi-modal microstructure.

RTP process is a complex three-dimensional deformation process, and the cost of research using experimental methods is very high. With the development of numerical simulation technology, finite element model (FEM) has become an important tool for simulating the RTP process and its formation. FEM dramatically reduces the required number of test cycles and simplifies the followings: the development of new techniques, research on tube-forming theories, forecasts of model results, and the study of microstructure changes [14–17]. Zhao [18] discussed the influence of feed angle on the force and energy parameters by rigid plastic FEM. Also by using similar method, Yin [19] studied the effect of roll speed on rolling defects by FEM, and the concept of critical speed was put forward. Pater [20] established a three-dimensional FEM considering the thermal phenomena, and explored the influence of process parameters on the deviation of internal and external diameters. Sim [21] adopted the rigid viscoplastic FEM with intelligent remeshing technique to study the distribution of strain and temperature field. In addition, Ding et al. [22] analyzed the distributions of stress, strain, and temperature of AZ31 alloy by FEM, and the magnesium alloy seamless tube was successfully manufactured by RTP method. However, all the models did not consider the change of the plug temperature. In the process of piercing, the temperature of the plug changes greatly and can't be treated as the thermostat. In this paper, a new three-dimensional finite element model which takes into account the change of the plug temperature is established in this paper.

As a two phase alloy which consists of the alpha phase and beta phase, a lot of research about the analysis and characterization of Ti–6Al–4V alloy has been done by the predecessors. Ding [23] studied the effect of double directional solidification technique on the lamellar microstructure of Ti–Al–Nb alloys by means of TEM and SEM. Gao [24] reported the crystallographic orientation evolution of titanium alloy and its dependence on process parameters by electron backscatter diffraction (EBSD) examination. In addition, the XRD technology has been increasingly used for crystal structure analysis. For example, Jandaghi [25–27] explored the crystallographic transformations during constrained groove pressing (CGP) and post-rolling process. By measuring XRD patterns under different deformation paths and different heat treatment conditions, the slip planes were discussed in detail.

In the present study, the numerical and experimental results of TATWs production using RTP method are presented. On the basis of the 3D rigid-plastic FE model of RTP, the effect of process parameters on the rolling block and temperature rise is studied by the control variable method. Finally, the TATWs with bi-modal microstructure are manufactured by RTP method.

2. Theoretical analysis

2.1. *Definition of process parameters*

There are three types of rotary tube piercing method nowadays: disk-type, barrel-type, and cone-type, as shown in Fig. 1a. With the development of RTP process, the application of barrel roll and cone roll is more extensive than that of disk roll. Hayashi proposed that the rotary forging effect of barrel roll was stronger than that of cone roll. The rotary forging effect may be a cause of the initiation of inside bore defects. So, the cone roll is more suitable for forming less deformable material than the barrel roll. The relative position of cone roll is illustrated in Fig. 1b. From the kinematic point of view, the two rolls rotate in the same direction, and the billet does spiral movement under the action of rolls during the RTP process. When the billet passes through the plug, the billet is machined into a hollow tube. There are two important angles in the piercing process of cone roll, one is the feed angle α and the other is the cross angle β. The angle between the roll axis and the rolling line on the horizontal plane is called the feed angle α. Feed angle has a great influence on the piercing speed, and the forward speed of billet decreases with the decrease of feed angle. The angle between the roll axis and the rolling line on the vertical plane is called the cross angle β, which is peculiar to the cone roll. The other three important process parameters are roll speed W, reduction ε and plug advance against gorge C, respectively. During the RTP process, the roll speed and reduction have significant impact on temperature

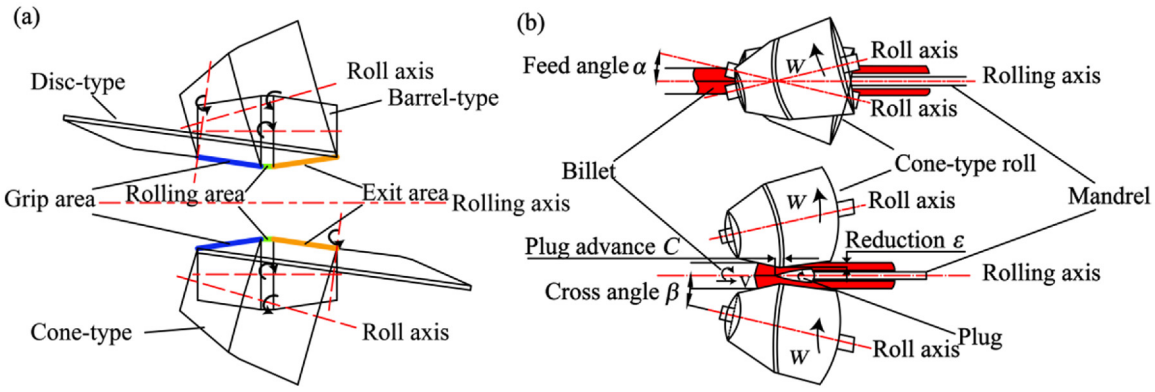

Fig. 1 – Three typical roll types in the RTP process are shown in (a), and (b) represents the die position of cone roll.

rise, and the plug advance against gorge determines the bite condition of the piercing process.

2.2. *Mechanical analysis*

Due to the narrow processing window of titanium alloy and small internal expansion of thick-walled tubes, there are two key problems in the application of the RTP method to the manufacture of TATWs with bi-modal microstructure: rolling block and severe temperature rise.

The phenomenon of rolling block is that the billet is stuck in the middle of the roll, which is caused by the resistance of the billet greater than the driving force. Accordingly, it is necessary to discuss the mechanical conditions of billet. During the RTP process, the force analysis of the billet is shown in Fig. 2. The billet is affected by three forces, friction of roll T, positive pressure of roll P and resistance of plug nose Q'. The orthogonal decomposition of these three forces shows that the axial component of T_x is the driving force, and the axial component of P_x and Q' are the resistance forces. Whether the piercing process can be completed smoothly depends on the relationship between these three forces. In this condition, the piercing process could be achieved smoothly:

$$2T_x \geq 2P_x + Q' \tag{1}$$

In this condition, the piercing process could not be achieved;

$$2T_x > 2P_x + Q' \tag{2}$$

where T_x and P_x are mainly affected by the reduction rate; Q' is determined by the plug nose pressure and area. When the plug dimension is determined, Q' is a single valued function of the plug nose pressure:

$$Q' = \pi r_H^2 p_H \tag{3}$$

where P_H, n_H and σ_s are the specific pressure of plug nose, stress state coefficient and yield stress, respectively. The specific pressure of plug nose is determined by the stress state of billet and yield stress, and the different process parameters correspond to different stress states:

$$p_H = n_H \sigma_S \tag{4}$$

Substituting Eqs. (3) and (4) into Eq. (2), the new bite condition of RTP process is obtained:

$$2(T_x - P_x) \geq \pi r_H^2 n_H \sigma_S \tag{5}$$

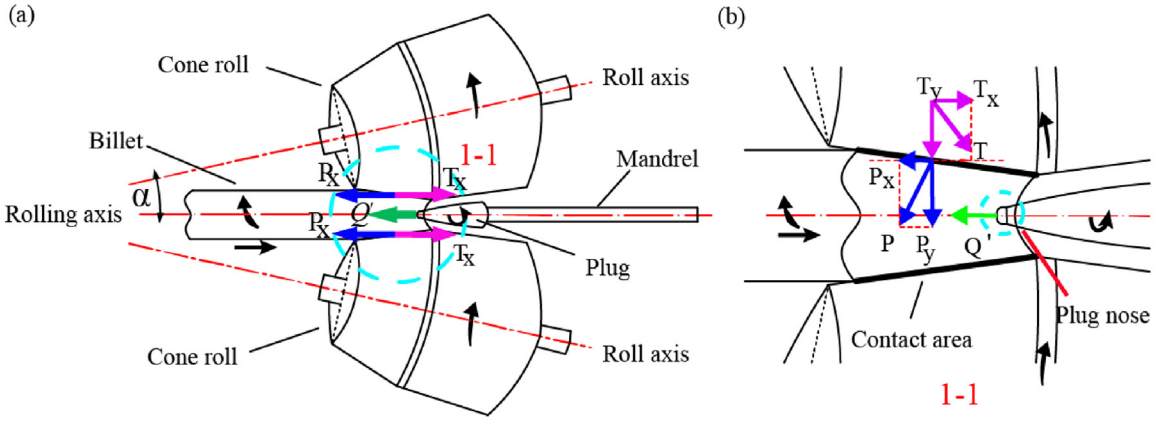

Fig. 2 – A schematic diagram of (a) the axial force indication of the billet and (b) stress decomposition during the RTP process.

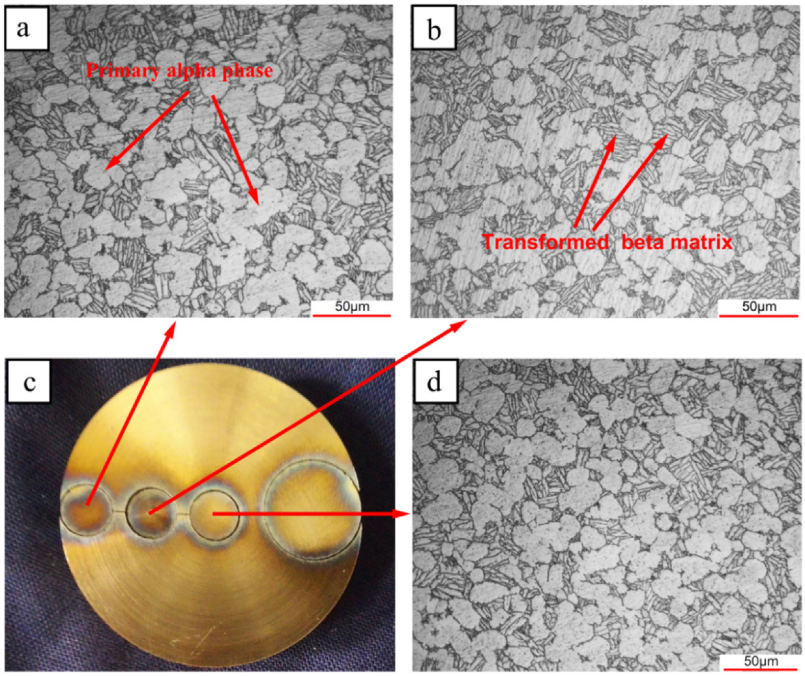

Fig. 3 – Optical micrograph map of the original billet in different positions: (a) surface layer, (b) transition layer, (c) sample, and (d) central layer..

Therefore, by adjusting the different process parameters, the bite conditions of the piercing process can be changed to solve the rolling block phenomenon in the piercing process of TATWs.

2.3. *Thermodynamic analysis*

Another key problem of the RTP process is the severe temperature rise. During the RTP process, there are two main aspects of heat generation: friction heat and deformation heat. The friction heat is mainly related to the friction stress and the relative sliding between the deformed body and the die [28]:

$$Q = \mu F_n v \tag{6}$$

where Q, μ, F_n and v are the friction heat, heat distribution coefficient, friction stress and relative sliding between the deformed body and the die, respectively. The deformation heat is mainly affected by the equivalent stress and the equivalent strain rate [29]:

$$\dot{S} = \alpha \bar{\sigma} \dot{\bar{\epsilon}} \tag{7}$$

where $\dot{S}$, α $\bar{\sigma}$ and $\dot{\bar{\epsilon}}$ are the heat-generation rate due to plastic deformation, thermal conversion efficiency, equivalent stress and the equivalent strain rate, respectively. Therefore, all the technological parameters which are beneficial to reduce the friction heat and deformation heat are advantageous to control the temperature rise.

However, the rolling block and the severe temperature rise are mutually restrictive during the RTP process. When the low deformation temperature is adopted, the phenomenon of rolling block is easy to appear because of the higher resistance of titanium alloy. Correspondingly, when the high deformation temperature is adopted, the optical micrograph map of the pierced tube is often widmanstatten microstructure. What's more, the reduction rate and roll speed also have a great influence on the process of RTP. Therefore, reasonable control of the thermal parameters is the key to obtain TATWs with bi-modal microstructure.

3. Numerical modeling of the RTP process

The characteristics of highly nonlinearity, periodic loading, and complex thermal process parameters change exist during the RTP process. Especially highly nonlinearity which comprises geometry nonlinearity, material nonlinearity, and contact nonlinearity have significant effect on RTP process. Thus, based on the basic principle of RTP, an efficient and reliable finite element model is established to study the effect of thermal parameters on the piercing process.

3.1. *Material model*

The material of the billet is Ti–6Al–4V which has a narrow processing window. The original billet is a cylindrical bar with diameter of 50 mm obtained by the cogging process, and the β_t which was measured by the metallographic observation method is $1000 \pm 5\,^{\circ}C$. The microstructure of the billet distributes uniformly, which is composed of primary alpha phase, lamellar alpha phase and beta matrix, as shown in Fig. 3. The content of primary alpha phase is counted by the

Table 1 – Statistics of alpha phase in different positions.

Position	Primary alpha phase content (%)	Diameter of primary alpha phase (μm)	Width of lamellar alpha phase (μm)
Surface layer	43.05	19.65	2.50
Transition layer	44.23	21.32	2.53
Central layer	43.93	20.46	2.52

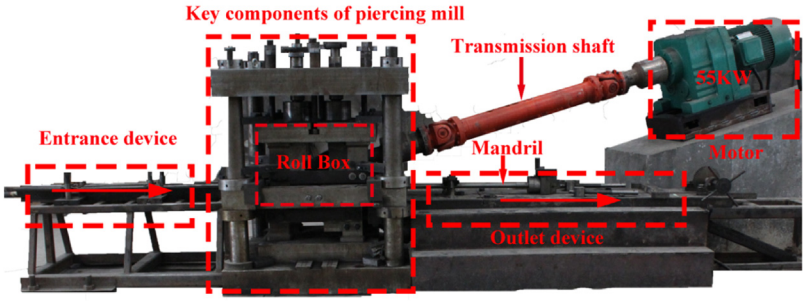

Fig. 4 – Self-developed machine for RTP used in the experiments.

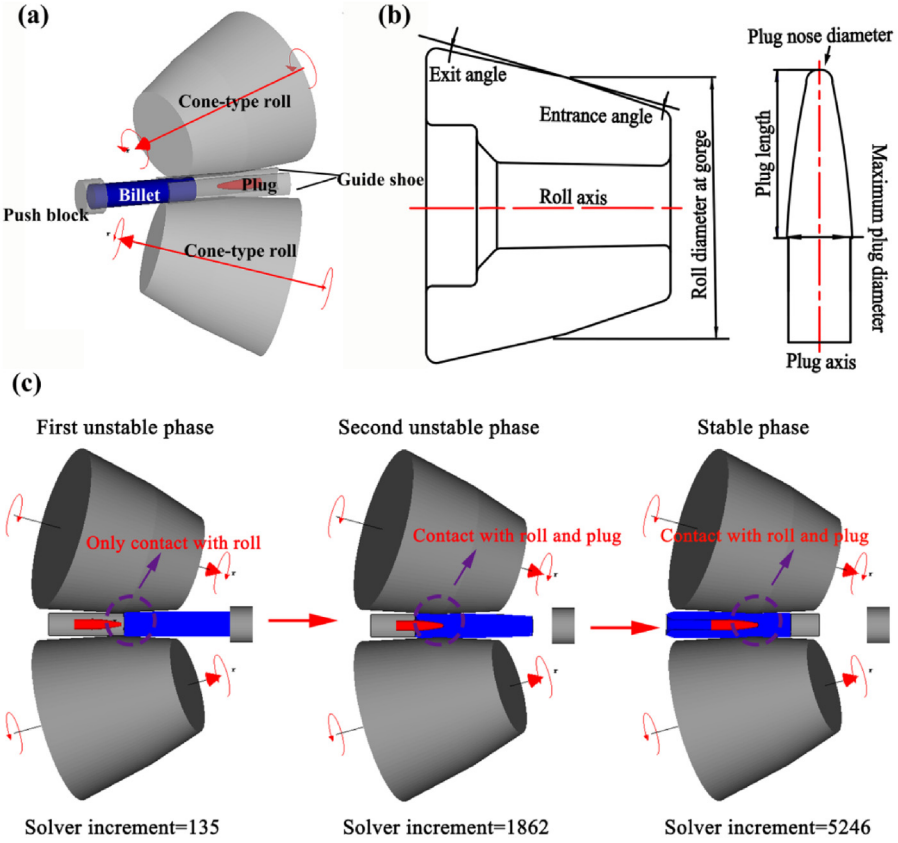

Fig. 5 – The geometric model and typical piercing states: (a) FEM model, (b) shapes of the roll and plug, (c) three typical states of RTP process.

software of Image-Pro Plus (IPP), and the statistical results are shown in Table 1. The average content of primary alpha phase is about 43.74%, and the width of the lamellar alpha phase is about 2.52 μm. The flow stress curves of Ti–6Al–4V alloy were obtained by the isothermal compression experiment, which was conducted on Gleeble-3500 thermal mechanical simulator. The ranges of experimental temperature and strain rate are 900–1020 °C and 0.001–50 s^{-1}, respectively. The flow stress

Table 2 – Specifications of the roll and plug.

Parameter	Value
Roll diameter at gorge (mm)	240
Entrance angle (°)	3
Exit angle (°)	3
Plug length (mm)	50
Maximum plug diameter (mm)	20
Plug nose diameter (mm)	3.5

Table 3 – Process parameters of RTP.

Parameter	Value
Billet diameter (mm)	45
Temperature (°C)	940–960
Guide space (mm)	46–51
Reduction rate (%)	4–16
Feed angle (°)	8–15
Cross angle (°)	15
Roll speed (rpm)	30–90
Plug advance against gorge (mm)	10

curve obtained by the experiment was introduced into the finite element analysis software to establish the material model of Ti–6Al–4V alloy, and other thermal physical parameters of Ti–6Al–4V alloy were taken from the literature [30]. What's more, the material of the roll and plug is 5CrNiMo and ultra-high strength steels (C250), respectively.

3.2. *Experimental equipment*

According to the forming characteristics of less deformable alloys, a new piercing mill of cone roll is designed, as shown in Fig. 4. The piercing mill consists of four main parts, entrance device, key components of piercing mill, outlet device and motor. The main function of the entrance device is to accurately locate the location of billet to realize the first bite process. The key components of piercing mill are composed of two cone rolls, two guide shoes, push block, and plug, as shown in Fig. 5a. Its main role is to transform solid billet into hollow tube. Fig. 5b shows the shape of the roll and plug, and the specifications of the roll and plug are shown in Table 2. What's more, the outlet device is mainly designed to accomplish the positioning of mandrel. During the RTP process, the two rolls continuously rotate around their axis under the drive of the motor. Simultaneously the billet goes along the rolling line under the action of push block. When the billet enters the deformation region, the RTP process is smoothly established, as shown in Fig. 5c.

3.3. *Boundary condition*

In addition to the equipment model and material model, the treatment of boundary condition also has tremendous influence on the simulation accuracy. In the finite element model, the temperature of the rolls is set as 25 °C. The plug is meshed and the initial temperature is also set as 25 °C. The heat exchange process between the billet and the dies is simulated by defining the heat transfer coefficient. In addition, the time step of the simulation process should be less than the mesh size of the billet to ensure the calculation precision. The hexahedral mesh of the billet is 3 mm, and the step length of the roll is 1 mm. The process of forming Ti–6Al–4V alloy thick-walled tubes by RTP method includes the following three steps: adjustment of equipment parameters, billet heating and piercing which is carried out on self-developed piercing mill. The main process parameters are shown in Table 3.

4. Results and discussion

4.1. *Results of simulation*

In order to explore the feasibility of manufacturing TATWs by RTP method, the distribution law of field variables in this process was investigated by the FEM software. Fig. 6 displays the three different stages of RTP. During the first bite process, the billet moves along the rolling line in a spiral way, and the diameter of the billet decreases gradually, as shown in Fig. 6a. The plastic deformation of billet is mainly concentrated in the surface layer. When the billet encounters the plug, the inner hole of tube begins to appear, as shown in Fig. 6b. During the second bite process, the billet is fully rolled under the combination action of roll and plug. The plastic deformation increased gradually in all parts of the billet. With the deformation continues, the inner hole of tube

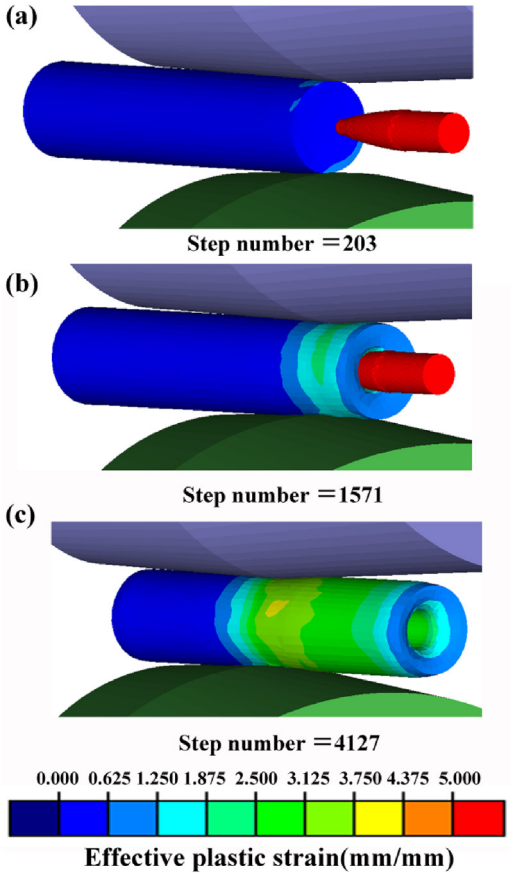

Fig. 6 – Different stages of the RTP process with the effective strain distribution indicated (a) first bite process, (b) second bite process, (c) steady piercing.

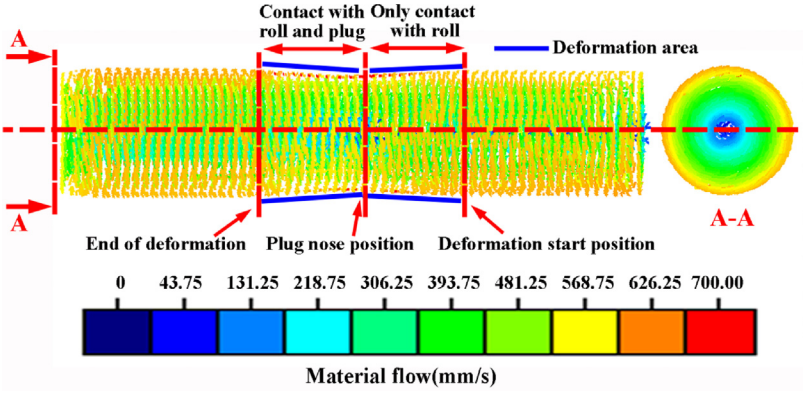

Fig. 7 – Material flow distribution of the RTP process during steady piercing stage.

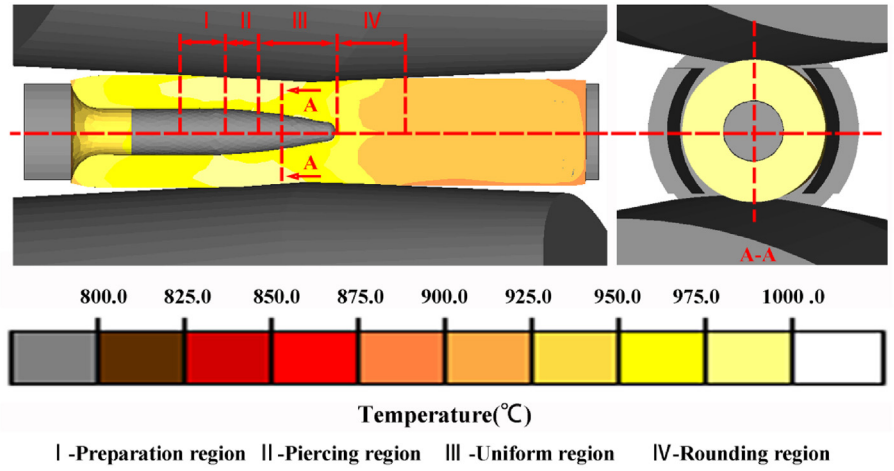

Fig. 8 – Temperature distribution of the RTP process during steady piercing stage.

expands gradually. When the billet completely wrapped plug, the piercing process reaches stable conditions, as shown in Fig. 6c.

With the aid of FEM, the material flow of the billet during the RTP process can be clearly displayed. The distribution of material flow during steady piercing stage is shown in Fig. 7. In the same cross section, the material flow velocity decreases gradually from the surface layer to the central layer under the action of rolls and plug. At the same time, the material flow velocity of surface layer in the longitudinal section is not consistent, which is the cause for the formation of torsional deformation during the RTP process. In general, the torsion deformation increases with the increase of the axial velocity difference.

The distribution of temperature during steady piercing stage is shown in Fig. 8. In the preparation region, there is a small temperature drop in the center of the billet after air cooling. The temperature of the piercing region is the highest under the action of deformation heat and friction heat. It is known from the A-A section that the temperature distribution in the cross section of the piercing area is uniform. What's more, the temperature of the head and tail is lower than that of middle part due to the heat exchange between the billet and the air.

During the RTP process, the entire volume of the material was intensively utilized, which is demonstrated by the distribution of effective plastic strain in Fig. 9. The highest effective plastic strain occurred in the surface layer of the pierced tubes due to the direct rolling of the roll. In the longitudinal section, the effective plastic strain presents a ''W'' type distribution at the front of plug. This indicates that the deformation is gradually permeated from the surface and center to the transition layer at the preparation region. In addition, the effective plastic strain of the surface and central layer is slightly larger than the transition layer under the action of the roll and the plug in the same cross section.

During the rotary rolling process, the Z direction of billet is affected by the roll pressure, and the corresponding tensile stress will be produced on the X direction, as shown in Fig. 10a. The value of the additional tensile stress directly determines whether the piercing process can be carried out smoothly. Therefore, it is necessary to study the influence of the reduction rate on the additional tensile stress. The additional tensile stress varies with the rolling process, as shown in

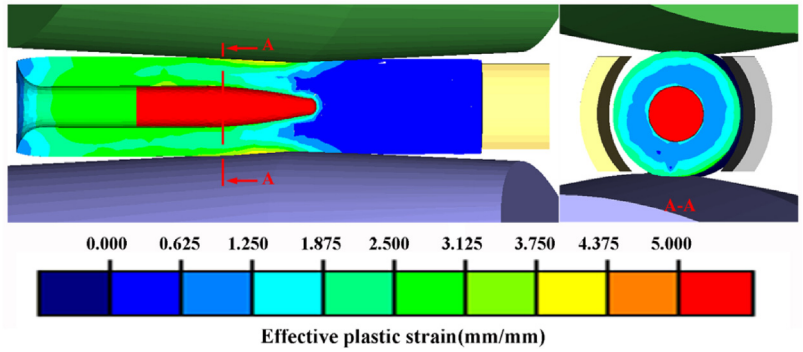

Fig. 9 – Effective plastic strain distribution of the RTP process during steady piercing stage.

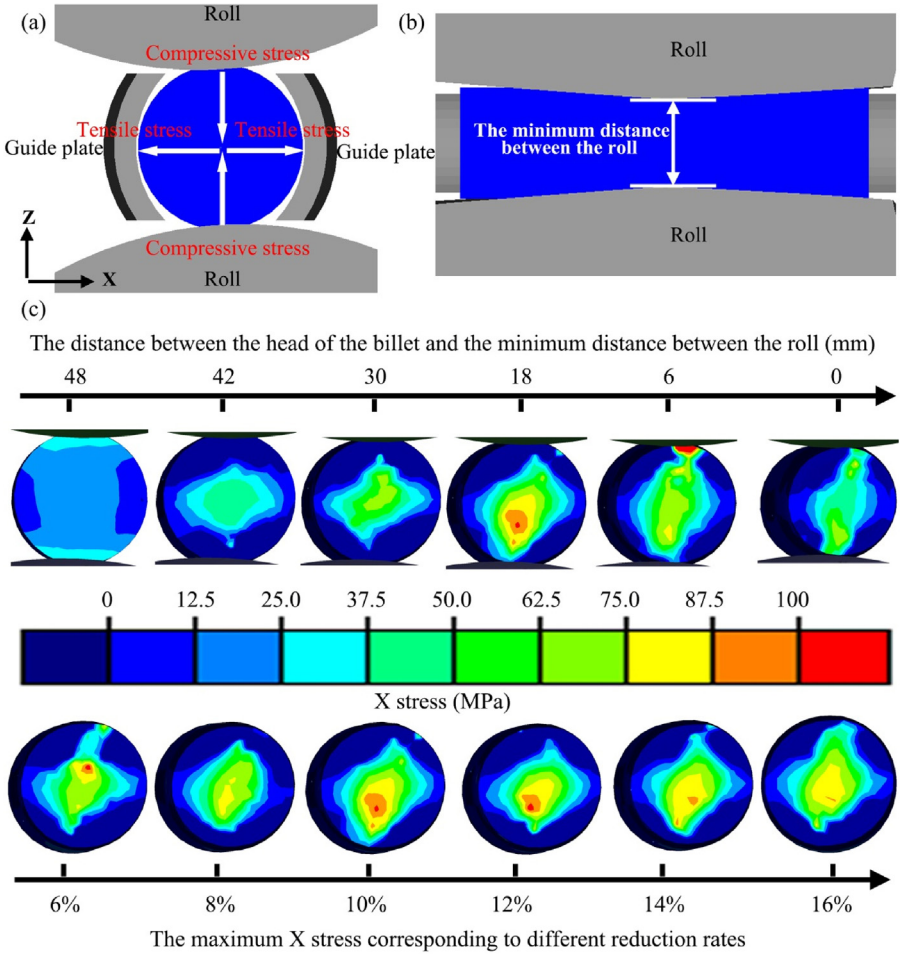

Fig. 10 – The principle of RTP process, (a) the additional tensile stress, (b) sketch map of the distance between rolls, (c) the evolution law of X stress and the maximum X stress corresponding to different reduction rates.

Fig. 10c. As the deformation extent increases, the additional tensile stress increases first and then decreases. By comparing the additional tensile stress under different reduction rates, it is found that the additional tensile stress first increases and then decreases with the increase of reduction rate. The reasonable reduction rate corresponding to the maximum tensile stress is within 10–16%.

4.2. *Verification of simulation and experimental results*

In order to verify the accuracy of the finite element model, the experiment of RTP was carried out on the self-developed piercing mill. It is obtained from Eq. (7) that the deformation heat is greatly influenced by the strain rate and effective stress. Hence, the piercing temperature and the reduction rate adopt a gradual

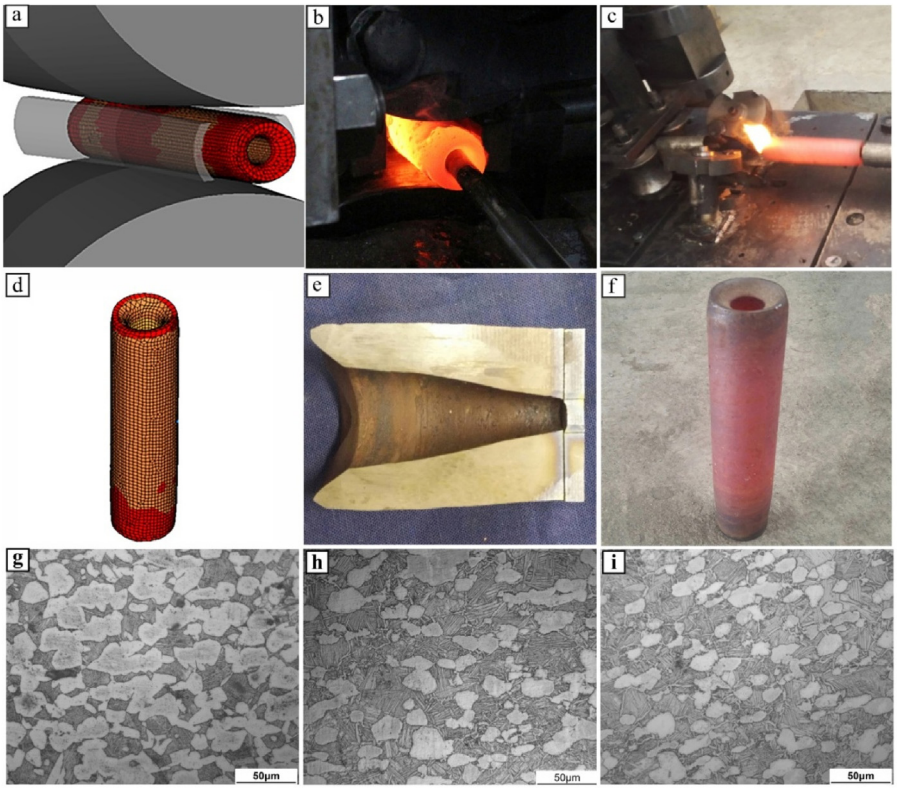

Fig. 11 – Experiment and simulation results of RTP process under different thermal parameters, (a) simulation process, (b) rolling block process, (c) smooth process, (d) tube obtained by simulation, (e) blocking sample obtained by experiment, (f) tube obtained by experiment, (g) microstructure of case 2, (h) microstructure of case 6, (i) microstructure of case 10.

Table 4 – Experiment and simulation results of RTP process under different thermal parameters.

	Temperature (°C)	Feed angle (°)	Reduction rate (%)	Roll speed (rpm)	Experiment result	Simulation result
1	940	15	4.0	60	Rolling block	Rolling block
2	940	15	6.0	60	Rolling block (pierced 30 mm)	Rolling block (pierced 50 mm)
3	960	15	4.0	60	Rolling block	Rolling block
4	960	15	6.0	60	–	Success
5	960	15	7.0	60	Success (serious wear of plug)	Success (temperature increase compared with case 4)
6	960	15	8.0	60	Success (slight wear of plug)	Success (temperature increase compared with case 5)
7	960	15	10	60	Success (no wear of plug)	Success (temperature increase compared with case 6)
8	960	15	8.0	30	–	Success (temperature decrease compared with case 6)
9	960	15	8.0	90	–	Success (temperature increase compared with case 6)
10	960	8	10	60	–	Success
11	960	8	12	60	Success (better surface quality)	Success

increasing method to select the reasonable thermal parameters. When the experiment temperature is set as 940 °C, the rolling block phenomenon often occurs due to the large deformation resistance of Ti–6Al–4V alloy, as shown in Fig. 11b and e. When the experiment temperature is increased into 960 °C and reduction rate increased into 7.0%, the piercing process was completed successfully, as shown in Fig. 11c and f. The simulation results of smooth piercing process are shown in Fig. 11a and d. On this basis, the piercing results under other process parameters are explored, and the predicted results are in a good agreement with the experimental results, as shown in Table 4. The simulation results show that the risk of the billet temperature exceeding the β_t increases sharply when the roll speed and the reduction rate continue to increase. At the same time, the experiment results show that the reduction rate has significant impact on the wear of plug. With the increase of the reduction rate, the wear of plug is weakened, and the rolling block phenomenon is gradually disappearing. The wear

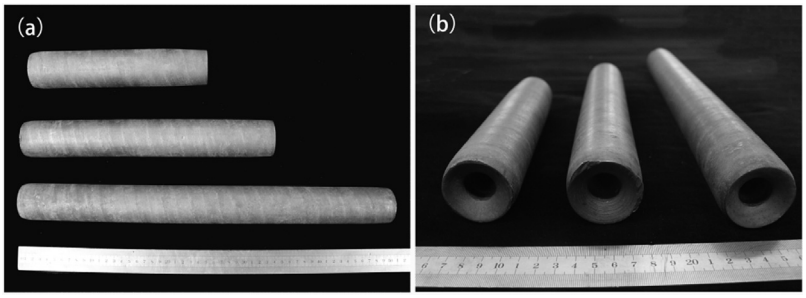

Fig. 12 – Axial and radial dimensions of various specifications: (a) axial dimension, (b) radial dimension.

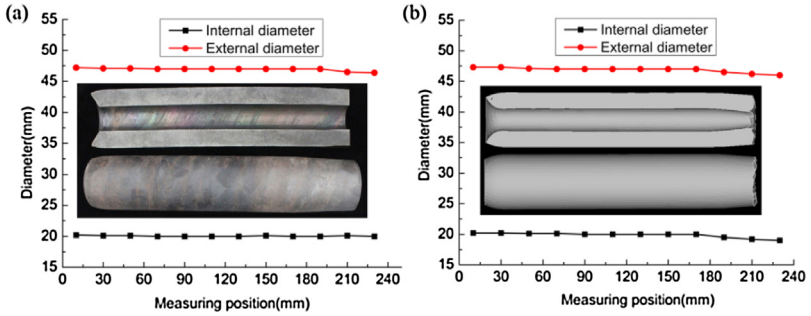

Fig. 13 – The comparisons of geometric dimensions between (a) experiment result and (b) simulation result.

condition of the plug is related to the pressure of the plug nose. Within a certain range, the additional tension stress of the billet center increases as the reduction rate increases. In general, the greater the additional tension stress, the smaller the pressure in the plug nose, and the smaller the wear of plug. In addition, compared with the feed angle equal to 15°, the surface quality of TATWs is better when the feed angle is equal to 8°.

The optical micrograph maps of the pierced tube under different process parameters are shown in Fig. 11g, h and i. The sample location is at $t/2$ of the steady deformation zone, and t represents wall thickness of the tube. The experimental results show that the deformation temperature has great influence on the content of primary alpha phase. With the increase of temperature, the content of primary alpha phase decreases. At the same time, under the combined action of reduction rate and feed angle, the primary alpha phase in case 10 is not significantly reduced.

The TATWs with various geometric dimensions are shown in Fig. 12. The surface of the TATWs is well, and the quality defects such as fold and crack are not found. At the same time, the tube is cut along the axis, and its internal diameter and external diameter are counted. The predicted dimensions are in a good agreement with the measured ones, as shown in Fig. 13. Accordingly, the piercing process can be used to manufacture TATWs with accurate dimensions.

4.3. *Microstructure distribution of the pierced tube*

In order to study the microstructure uniformity, samples are taken form head, middle and tail of the pierced tube, respectively, as shown in Fig. 14. The microstructure of the pierced tube is evenly distributed with bi-modal microstructure. At the same time, Ti–6Al–4V is a two phase alloy which consists of the alpha phase and beta phase. Compared with the beta phase of body-centered cubic structure, plastic deformation is difficult to occur in the primary alpha phase of close-packed hexagonal structure. However, the primary alpha phase of TATWs is elongated along the axil. This indicates that there is strong shear stress in the piercing process, which is beneficial to the plastic deformation of metal.

The SEM image was obtained to study the effect of deformation on each constituted phase, as shown in Fig. 15. Under the action of circumferential tensile deformation, some of the primary alpha phases are gradually elongated. The length-width ratio of these primary alpha phases is greater than 1, and shows certain directivity. However, the equiaxed primary alpha phase can also be observed in the pierced tube. The main reason for this phenomenon may be related to the globularization process of lamellar alpha phase induced by the severe shear strain. Further investigations are still necessary to provide the evidence of globularization mechanism. The beta phase plays a coordinating role in the plastic deformation process, and its microstructure is related to the precipitation process of lamellar alpha phase.

In the air cooling process after deformation, the lamellar alpha phase will be precipitated in the beta matrix of TC4 alloy. The shape and width of the lamellar alpha phase have great influence on the fatigue properties and the resistance of crack propagation. As shown in Fig. 14, the width of the lamella alpha phase in the middle part of the tube is larger than that in the other parts, due to the smaller cooling speed. Under the

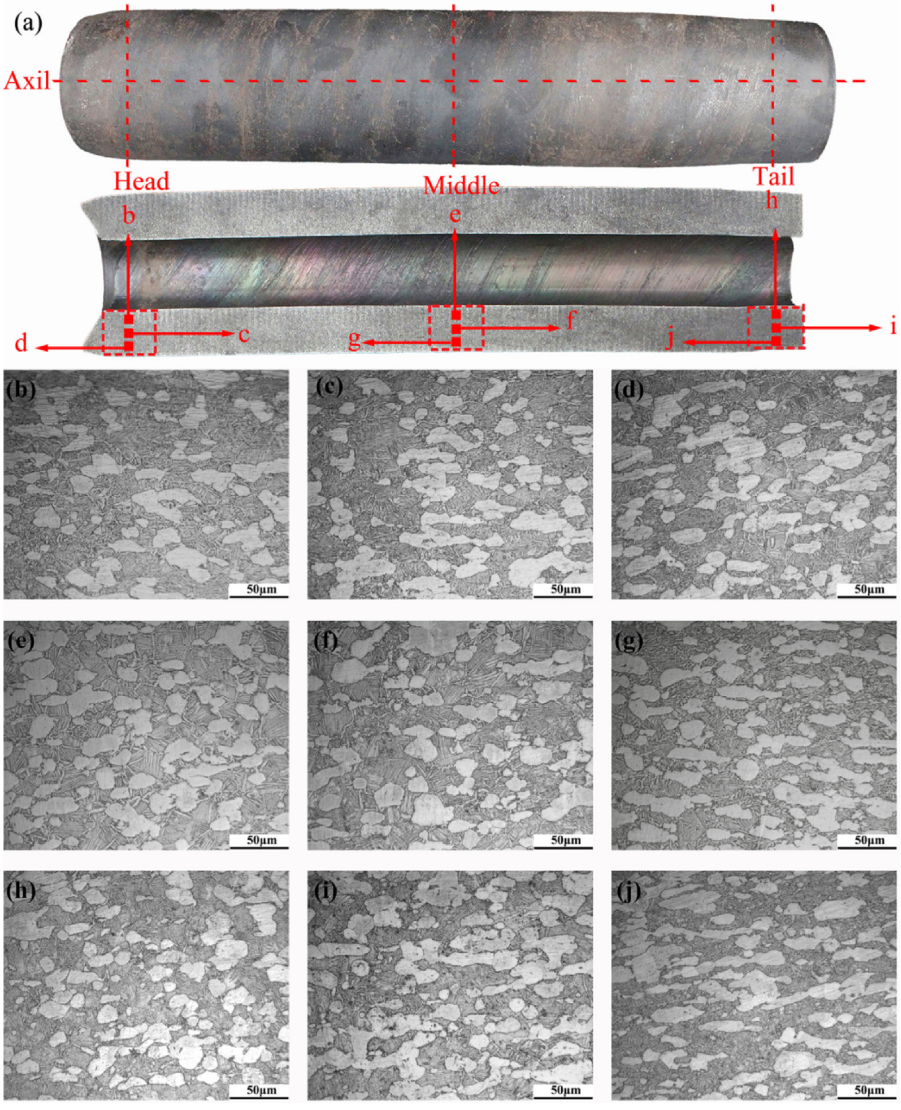

Fig. 14 – Optical micrograph map of the pierced tube correspondent to points (b)–(j).

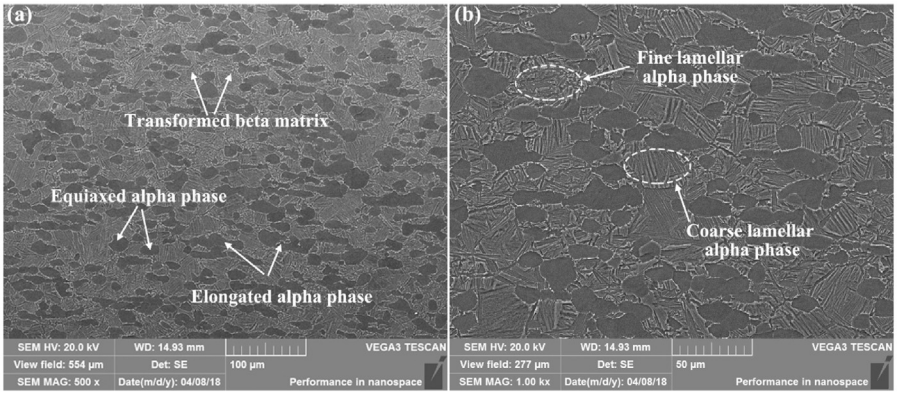

Fig. 15 – SEM image of the pierced tube corresponding to point f in Fig. 14, (a) 500×, (b) 1000×.

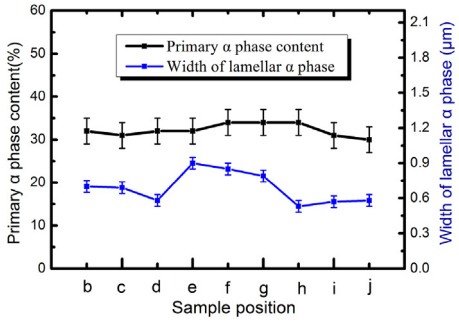

Fig. 16 – The content of primary alpha phase and the width of lamellar alpha phase correspondent to points (b)–(j) in Fig. 14, respectively.

combined deformation of compression and torsion, most of the lamellar alpha phases at beta boundaries are broken, which leads to the difference between lamellar alpha phases on beta boundaries and inside beta grain is small. In addition, both fine lamellar alpha phase and coarse lamellar alpha phase can be observed in the beta matrix, which is related to the deformation compatibility of beta phase, as shown in Fig. 15b.

The content of the primary alpha phase and the thickness of the lamellar alpha phase are counted by IPP software, and the results are shown in Fig. 16. The average content of the primary alpha phase in different sample position is about 32%, which is consistent with the distribution of temperature. It indicates that the temperature at the end of piercing deformation is lower than the β_t (1000 ± 5 °C). The width of the lamellar alpha phase is about 0.68 μm which is smaller than the initial microstructure. In addition, the difference of statistical results at each sample position is small, which is in agreement with the simulation results of the temperature field and the strain field. The variance of primary alpha phase is 0.0002, and the variance of lamellar alpha phase thickness is 0.016. Therefore, adopting the new method of RTP for TATWs production fully satisfied the microstructure requirements.

5. Conclusions

In the present work, a reliable 3D FE model of the RTP process was developed. The formation laws of RTP process were analyzed comprehensively by numerical and experimental method. The orientation study demonstrated that the RTP process is technically feasible for the production of TATWs with bi-modal microstructure. The conclusions are summarized as follows:

(1) During the rotary rolling process, the additional tensile stress reaches the maximum value before the minimum distance between rolls. With the increase of the reduction rate, the additional tensile stress first increases and then decreases. The reduction rate corresponding to the maximum tensile stress is within 10–16%.
(2) The reduction rate has significant impact on the rolling block phenomenon. In order to ensure the smooth progress of piercing process, the reduction rate should be greater than or equal to 6%.
(3) The simulation results show that the roll speed has significant impact on the temperature rise. With the increase of the roll speed the temperature rise of piercing is increased. The reasonable roll speed for the preparation of TATWs is 30–60 rpm.
(4) The microstructure of the pierced tube is evenly distributed with bi-modal microstructure, which consists of primary alpha phase surrounded by thin alpha platelets. The average content of the primary alpha phase is about 32%, and the variance is 0.0002. The width of the lamellar alpha phase is about 0.68 μm, and the variance is 0.016.

Acknowledgements

This work was supported by the National Natural Science Foundation of China (No. 51504195); the Fundamental Research Funds for the Central Universities (No. 3102016ZB043) and Shaanxi key research and development program (No. S2017-ZDYF-ZDXM-GY-0115).

REFERENCES

[1] M. Salem, M. Heydari, A new approach in modeling of guide and conical rolls in the ring rolling process, Int. J. Adv. Manuf. Technol. 81 (2015) 1831–1843.
[2] K.H. Lee, D.C. Ko, D.H. Kim, S.B. Lee, N.M. Sung, B.M. Kim, Control method for centering rolls in radial–axial ring rolling process, Int. J. Precis. Eng. Manuf. 15 (2014) 535–544.
[3] W.J. Zhang, X.Y. Song, S.X. Hui, W.J. Ye, Y.L. Wang, W.Q. Wang, Tensile behavior at 700 °C in Ti–Al–Sn–Zr–Mo–Nb–W–Si alloy with a bi-modal microstructure, Mater. Sci. Eng. A 595 (2014) 159–164.
[4] N. Kotkunde, A.D. Deole, A.K. Gupta, S.K. Singh, B. Aditya, Failure and formability studies in warm deep drawing of Ti–6Al–4V alloy, Mater. Des. 60 (2014) 540–547.
[5] W. Zhang, X. Jiao, Y. Yu, J. Yang, Y. Feng, Microstructure and properties of 3.5 vol.% TiBw/Ti6Al4V composite tubes fabricated by hot-hydrostatic extrusion, J. Mater. Sci. Technol. 30 (2014) 710–714.
[6] C. Wang, H.J.M. Geijselaers, E. Omerspahic, V. Recina, A.H. van den Boogaard, Influence of ring growth rate on damage development in hot ring rolling, J. Mater. Process. Technol. 227 (2016) 268–280.
[7] V.P. Romanenko, D.V. Sizov, Evaluating the adequacy of a mathematical model of the piercing of a billet into an ultra-thick-walled shell on a two-high rotary rolling mill, Metallurgist 57 (2014) 830–836.
[8] Y.Q. Zhao, J.H. Mao, F.F. Liu, Z.H. Ma, Experiments and simulation on mannesmann piercing process in the drill steel manufacture, Strength Mater. 47 (2015) 29–40.
[9] M.M. Skripalenko, V.E. Bazhenov, B.A. Romantsev, M.N. Skripalenko, T.B. Huy, Y.A. Gladkov, Mannesmann piercing of ingots by plugs of different shapes, Met. Sci. J. 32 (2016) 1712–1720.
[10] P.F. Bariani, S. Bruschi, A. Ghiotti, Advances in predicting damage evolution and fracture occurrence in metal forming operations, J. Manuf. Process. 14 (2012) 495–500.

[11] F. Liu, Y.L. Qiu, Z.H. Song, S.W. Wang, Numerical simulation of the piercing process of large-sized seamless steel tube, Appl. Mech. Mater. 319 (2013) 444–450.
[12] X. Yajing, X. Xianze, Z. Shuqi, D. Chao, Z. Jie, L. Mingqiang, TC4 titanium alloy seamless blooms made by rotary piercing, Rare Met. Lett. 1 (2008).
[13] P. Jiming, X. Yajing, Q. Henglei, D. Chao, M. Xiaoju, Y. Jianchao, J. Jianhui, Study on microstructure and properties of titanium and titanium alloy tube blanks manufactured by different methods, Titan. Ind. Prog. 4 (2010) 14.
[14] Y. Shuang, F. Wang, Q. Wang, Explorative study of tandem skew rolling process and equipment for producing seamless steel tubes, J. Mech. Eng. 214 (2017) 1597–1604.
[15] B. Du, C. Zhao, G. Dong, J. Bi, FEM-DEM coupling analysis for solid granule medium forming new technology, J. Mater. Process. Technol. (2017).
[16] H.H. Lee, J.I. Yoon, H.S. Kim, Single-roll angular-rolling: a new continuous severe plastic deformation process for metal sheets, Scr. Mater. 146 (2018) 204–207.
[17] Y. Li, J. Huang, G. Huang, W. Wang, J. Chen, Z. Zeng, Comparison of radial forging between the two-and three-split dies of a thin-walled copper tube during tube sinking, Mater. Des. 56 (2014) 822–832.
[18] Y.Q. Zhao, J.H. Mao, Effects of feed angle on mannesmann piercing in drill steel production, Adv. Mater. Res. 915–916 (2014) 996–999.
[19] Y. De Yin, M.J. Wang, S.Z. Li, P.Z. Wang, X.D. Wang, G.T. Li, Influence of roll rotational speed on inside bore and lamination defects in rotary piercing large diameter heavy wall P92 steel pipe process, Appl. Mech. Mater. 421 (2013) 205–211.
[20] Z. Pater, J. Bartnicki, J. Kazanecki, 3D finite elements method (FEM) analysis of basic process parameters in rotary piercing mill, Metalurgija 27 (2012) 257–263.
[21] S.H.S. Gyeongsang, J.M.C. Gnu, M.C.L. Gnu, Finite element analysis of a Mannesmann rollpiercing process, Proc. Jpn. Soc. Technol. Plast. 2 (2011) 515–516.
[22] X. Ding, Y. Shuang, Q. Liu, C. Zhao, New rotary piercing process for an AZ31 magnesium alloy seamless tube, Mater. Sci. Technol. 836 (2017) 1–11.
[23] X.F. Ding, J.P. Lin, L.Q. Zhang, Y.Q. Su, G.L. Chen, Microstructural control of TiAl–Nb alloys by directional solidification, Acta Mater. 60 (2012) 498–506.
[24] P. Gao, Y. Cai, M. Zhan, X. Fan, Z. Lei, Crystallographic orientation evolution during the development of tri-modal microstructure in the hot working of TA15 titanium alloy, J. Alloys Compd. 741 (2018) 734–745.
[25] M.R. Jandaghi, H. Pouraliakbar, G. Khalaj, M.J. Khalaj, A. Heidarzadeh, Study on the post-rolling direction of severely plastic deformed Aluminum–Manganese–Silicon alloy, Arch. Civ. Mech. Eng. 16 (2016) 876–887.
[26] H. Pouraliakbar, M.R. Jandaghi, S.J.M. Baygi, G. Khalaj, Microanalysis of crystallographic characteristics and structural transformations in SPDed Al Mn Si alloy by dual-straining, J. Alloys Compd. 696 (2017) 1189–1198.
[27] H. Pouraliakbar, M.R. Jandaghi, G. Khalaj, Constrained groove pressing and subsequent annealing of Al–Mn–Si alloy: microstructure evolutions, crystallographic transformations, mechanical properties, electrical conductivity and corrosion resistance, Mater. Des. 124 (2017) 34–46.
[28] B. Qiu, J. Li, Numerical investigations on the heat transfer behavior of brush seals using combined computational fluid dynamics and finite element method, J. Heat Transfer. 135 (2013) 122601.
[29] B. Fekete, A. Szekeres, Investigation on partition of plastic work converted to heat during plastic deformation for reactor steels based on inverse experimental–computational method, Eur. J. Mech. 53 (2015) 175–186.
[30] Y. Zheng, D. Liu, Y. Yang, Z. Zhang, X. Li, R. Zhang, Microstructure evolution of Ti–6Al–4V with periodic thermal parameters during axial closed die rolling process, J. Alloys Compd. 735 (2018) 996–1009.